MNRAS **000**, 1–15 (2017) Preprint 17 January 2017 Compiled using MNRAS LATEX style file v3.0

Constraints on the optical polarization source in the luminous non-blazar quasar 3C 323.1 (PG 1545+210) from the photometric and polarimetric variability

Mitsuru Kokubo,[1,2]⋆
[1] *Department of Astronomy, School of Science, the University of Tokyo, 7-3-1 Hongo, Bunkyo-ku, Tokyo 113-0033, Japan*
[2] *Institute of Astronomy, the University of Tokyo, 2-21-1 Osawa, Mitaka, Tokyo 181-0015, Japan*

arXiv:1701.03798v1 [astro-ph.GA] 13 Jan 2017

Accepted 2017 January 10. Received 2017 January 08; in original form 2016 November 29

ABSTRACT

We examine the optical photometric and polarimetric variability of the luminous type 1 non-blazar quasar 3C 323.1 (PG 1545+210). Two optical spectro-polarimetric measurements taken during the periods 1996−98 and 2003 combined with a V-band imaging polarimetric measurement taken in 2002 reveal that (1) as noted in the literature, the polarization of 3C 323.1 is confined only to the continuum emission, that is, the emission from the broad line region is unpolarized; (2) the polarized flux spectra show evidence of a time-variable broad absorption feature in the wavelength range of the Balmer continuum and other recombination lines; (3) weak variability in the polarization position angle (PA) of ~ 4 deg over a time-scale of 4−6 years is observed; and (4) the V-band total flux and the polarized flux show highly correlated variability over a time-scale of one year. Taking the above-mentioned photometric and polarimetric variability properties and the results from previous studies into consideration, we propose a geometrical model for the polarization source in 3C 323.1, in which an equatorial absorbing region and an axi-asymmetric equatorial electron-scattering region are assumed to be located between the accretion disc and the broad line region. The scattering/absorbing regions can perhaps be attributed to the accretion disc wind or flared disc surface, but further polarimetric monitoring observations for 3C 323.1 and other quasars with continuum-confined polarization are needed to probe the true physical origins of these regions.

Key words: accretion, accretion discs – galaxies: active – galaxies: nuclei – polarization – quasars: individual (3C 323.1)

1 INTRODUCTION

It has long been known that the ultraviolet(UV)-optical emission of non-blazar active galactic nuclei (AGNs) often shows weak linear polarization. The polarization observed in type 2 AGNs is considered to be the result of electron/dust scattering of the AGN nuclear emission from the polar scattering region; photons from the accretion disc and the broad line region (BLR) behind the obscuring dust torus are scattered into the observer's line of sight by the polar scattering region and, thus, the blue disc continuum and BLR emission appear in the polarized flux spectra (Antonucci & Miller 1985). Observations have revealed that the polarization position angle (PA) in type 2 objects is generally perpendicular to the radio jet structure (note that the jet axis is thought to be parallel to the accretion disc's rotation axis), as expected by the polar scattering model (e.g., Antonucci 1983; Brindle et al. 1990; Smith et al. 2004). On the other hand, in the case of type 1 AGNs with a prominent radio jet structure, polarization is generally known to be shown parallel to the radio structure (e.g., Stockman et al. 1979; Antonucci 1983; Stockman et al. 1984; Schmidt & Smith 2000; Smith et al. 2002; Kishimoto et al. 2004). Even for radio-quiet objects, high-spatial-resolution imaging observations have revealed there to be a significant correlation between the direction of the extended emission region (which is another good tracer of the accretion disc's rotation axis) and the polarization PA, in that the former tends to be parallel to the latter in type 1 objects and perpendicular in type 2

⋆ E-mail: mkokubo@ioa.s.u-tokyo.ac.jp

© 2017 The Authors

objects (Zakamska et al. 2005; Borguet et al. 2008). It is generally difficult to explain the "parallel" polarization observed in type 1 objects by the polar scattering or the polarization induced within the atmosphere of a plane-parallel scattering-dominated disc (e.g., Antonucci 1988; Kishimoto et al. 2003). In addition, some authors have claimed that the intrinsic quasar accretion disc continua must be completely depolarized because of the strong Faraday depolarization with magnetic fields in the disc atmosphere (Agol & Blaes 1996; Silant'ev et al. 2009, and references therein). Instead, the observed optical polarization properties in type 1 quasars can be understood by assuming a geometrically and optically thin equatorial electron-scattering region located inside the dust torus; photons produced inside this electron-scattering region can be scattered into our line of sight, resulting in a net linear polarization "parallel" to the disc rotation axis (e.g., Stockman et al. 1979; Antonucci 1988; Smith et al. 2004, 2005; Goosmann & Gaskell 2007; Kishimoto et al. 2008a; Batcheldor et al. 2011; Gaskell et al. 2012; Marin & Goosmann 2013; Hutsemékers et al. 2015; Silant'ev et al. 2016). It is currently believed that all AGNs/quasars have both equatorial and polar scattering regions, and that differences in the observed polarization properties between type 1 and type 2 objects are due to the orientation effect (e.g., Smith et al. 2004).

In most type 1 Seyfert galaxies, it is observationally known that not only are the UV-optical continua polarized but also the BLR emission lines. polarization of the BLR emission lines is often observed to be at a lower polarization degree and a different PA than the continuum emission, and the rotation of the PA can be seen as a function of the wavelength (e.g., Smith et al. 2002, 2004) This implies that the equatorial electron scattering region is more or less similar in size to the BLR in these AGNs (e.g., Angel & Stockman 1980; Smith et al. 2005; Kishimoto et al. 2008a; Baldi et al. 2016). However, optical spectro-polarimetric observations for luminous type 1 quasars[1] with "parallel" optical polarization carried out by Antonucci (1988), Schmidt & Smith (2000) and Kishimoto et al. (2003, 2004, 2005, 2008b) have revealed that there is a population of quasars whose BLR emission lines are essentially unpolarized, i.e., the polarization of these quasars is confined only to the continuum. The observed null polarization of the BLR emission rules out the possibility that the optical polarization in these quasars is predominantly attributed to scattering processes outside the BLR (e.g., Smith et al. 1993; Kishimoto et al. 2003). The continuum polarization PAs of these quasars are mostly wavelength-independent, indicating that there is a single dominant mechanism producing the observed polarization.

Kishimoto et al. (2003, 2004) interpreted the continuum-confined polarization observed in several type 1 quasars such that the equatorial electron scattering region in these quasars is smaller in size compared to the BLR, but still much larger than the UV-optical emitting regions of the accretion disc. In such a geometrical configuration, electron scattering produces no net polarization in the observed BLR emission because the polarization is cancelled out when the polarized BLR flux vectors are averaged over a wide range of angles, and thus the polarization due to equatorial electron scattering is confined only to the accretion disc continua (see also Kishimoto et al. 2008a). One interesting consequence of Kishimoto's interpretation is that because the electron (Thomson) scattering cross-section is wavelength-independent, the polarized flux spectra in these quasars should reflect the spectral shape of the intrinsic accretion disc continua hidden under the strong BLR emission (Antonucci 2002; Kishimoto et al. 2003, 2004; Hu & Zhang 2012; Marin & Goosmann 2013). Interestingly, Kishimoto et al. (2004) showed that the polarized flux spectra of quasars with continuum-confined polarization share a similar spectral break feature at $\lambda_{\rm rest} \sim 3600$Å, which they interpreted as the Doppler-broadened hydrogen Balmer absorption edge imprinted in the intrinsic accretion disc thermal emission due to the disc atmospheric opacity effect. Kishimoto et al. (2004) further claimed that the overall spectral shape of these quasars (including the Balmer edge-like spectral break) can be well described by the non-local thermodynamic equilibrium radiative-transferred thermal accretion disc model of Hubeny et al. (2000) (see also Hu & Zhang 2012).

However, Kokubo (2016) has pointed out that the spectral shape of the accretion disc continua of quasars with continuum-confined polarization revealed as the variable component spectra (see Section 2.1) contradicts that revealed as the polarized component spectra, which may imply that equatorial electron scattering of the disc continua alone probably cannot explain the optical polarization properties in these quasars. Moreover, it should be noted that, before the deep spectro-polarimetric observations conducted by Kishimoto et al. (2004), Schmidt & Smith (2000) had carried out spectro-polarimetry for quasar samples overlapping with those used by Kishimoto et al. (2004) and suggested that the polarization in quasars with continuum-confined polarization may be attributed to a weak optical synchrotron component from the misdirected blazar core components. In fact, all of the five quasars (3C 323.1, Ton 202, B2 1208+32, 3C 95, and 4C09.72) confirmed as showing continuum-confined polarization by both Schmidt & Smith (2000) and Kishimoto et al. (2004) are radio-loud objects; thus, it is unsurprising that there is a flux contribution from the jet synchrotron component to the observed optical spectra (see e.g., Impey et al. 1989; Smith et al. 1993 and Afanasiev et al. 2015 for the cases of 3C 273 and 3C 390.3). However, it should be noted that subsequent work by Kishimoto et al. (2008b) has identified two radio-quiet quasars (Q0144-3938 and CTS A09.36) with continuum-confined polarization.

As discussed above, the optical polarization source in quasars with continuum-confined polarization has yet to be fully understood. To probe the true nature of the optical polarization mechanism, and consequently to examine the accretion disc physics in luminous type 1 quasars, detailed studies of the quasar polarimetric variability must be a key observable to constrain the geometry of the polarization source (e.g., Stockman et al. 1979; Schmidt & Smith 2000; Gallagher et al. 2005; Gaskell et al. 2012; Afanasiev et al. 2015; Rojas Lobos et al. 2016). In this work we examine the variability of the total flux, polarization degree, polariza-

[1] In this paper, we use the term "quasars" to refer to optically identified bright AGNs, including the radio-loud and the radio-quiet objects.

tion PA, and the polarized flux in the luminous type 1 non-blazar quasar 3C 323.1, which is a quasar with continuum confined polarization identified by Schmidt & Smith (2000) and Kishimoto et al. (2004), by collecting archival data.

The three polarimetry data sets used in this work, including the two optical spectro-polarimetric measurements taken by Schmidt & Smith (2000) (Bok/SPOL in 1996-1998) and by Kishimoto et al. (2004) (Keck/LRIS in 2003) and a V-band imaging-polarimetry measurement by Sluse et al. (2005) (ESO3.6-m/EFOSC2 in 2002), are described in Section 2. The absolute V-band magnitudes at the epochs of the spectro-polarimetric measurements are carefully estimated by using broad-band light curves taken from the literature. In Section 3, we first examine the spectral variability of the polarimetric properties between the two spectro-polarimetric measurements, and identify the origin of the different conclusions between Schmidt & Smith (2000) and Kishimoto et al. (2004) regarding the polarization source in the quasars with continuum-confined polarization described above. We then examine the V-band photometric and polarimetric variability of 3C 323.1 using all three polarimetric measurements in order to constrain observationally the geometry of the optical polarization source in 3C 323.1 in Section 4. Finally, a summary and conclusions are provided in Section 5.

2 DATA

Throughout this paper, we assume a cosmology of $H_0 = 73$ km/s/Mpc, $\Omega_m = 0.27$, and $\Omega_\Lambda = 0.73$ (Spergel et al. 2007). None of the data are corrected for Galactic extinction. In this study, "the total flux" (F_λ or F_ν) has the same meaning as the un-normalised Stokes parameter I expressed in units of the flux. q and u represent the normalised Stokes parameters defined as Q/I and U/I, whose polarization PA is defined using the equatorial coordinate system (a PA of 0 deg corresponds to North-South, and the PA increases from North towards East). The polarization degree $p \equiv \sqrt{q^2+u^2}$ obtained from the observational data with finite measurement errors[2] is known to be a biased estimate of the true polarization degree; therefore, the de-biased estimate of the polarization degree, $\hat{p} \equiv \sqrt{p^2-\sigma^2}$ (e.g., Plaszczynski et al. 2014), is used throughout this study. The rotated normalised Stokes parameters q' and u' are defined in a coordinate system rotated to the systemic polarization position angle PA_c of the target; note that all of the polarization, in principle, falls in the single Stokes parameter q' when the object has a wavelength-independent PA.

2.1 Observational properties of 3C 323.1: the variable component spectrum

3C 323.1 (PG 1545+210) is a Fanaroff-Riley II (FRII) radio-loud quasar at $z = 0.264$ (the luminosity distance $d_L = 1293.3$ Mpc; Wright 2006). The lobe-dominant radio jet structure of 3C 323.1 has a size of $\sim$ 300 kpc, and its position angle is $\sim$ 20 deg (Miley & Hartsuijker 1978; Kellermann et al. 1994; Dennett-Thorpe et al. 2000; Schmidt & Smith 2000; Kishimoto et al. 2004). As is the case with the other quasars with the continuum-confined polarization, the radio jet axis of 3C 323.1 is known to be parallel to the direction of the optical polarization vector within $\lesssim$ 10 deg (see Section 4; Stockman et al. 1979; Schmidt & Smith 2000; Kishimoto et al. 2004). In the optical wavelength range, 3C 323.1 is observed as a point source with an apparent V-band magnitude of $V \sim 16$ mag. The optical multi-band colour of 3C 323.1 is within the spectroscopic target selection criteria in the Sloan Digital Sky Survey (SDSS) Legacy Survey (Richards et al. 2002), meaning that this object is "normal" in terms of its optical spectrum (see also Boroson & Green 1992). The black hole mass (M_{BH}) and the Eddington ratio (defined as the ratio of the bolometric luminosity L to the Eddington luminosity L_E) of 3C 323.1 were estimated to be $\log(M_{\rm BH}/M_\odot) = 9.07$ and $L/L_E = 0.10$, respectively, based on the single-epoch SDSS spectrum obtained at MJD=53886 (Shen et al. 2011).

Recently, Kokubo (2016) has presented the multi-band (u, g, r, i, and z-band) photometric light curves for 3C 323.1 obtained in 2015-2016, and has examined the spectral shape of the UV-optical variable component spectrum in this object. Kokubo (2016) showed that the variable component spectrum in 3C 323.1 is consistent with a power-law spectrum with $\alpha_\nu \sim +1/3$ (in the form of $F_\nu \propto \nu^{\alpha_\nu}$). The spectral index of $\alpha_\nu \sim +1/3$ is commonly detected in the variable component spectra of (mostly radio-quiet) quasars (e.g., Pereyra et al. 2006; Ruan et al. 2014; Kokubo et al. 2014; MacLeod et al. 2016; Hung et al. 2016; Buisson et al. 2017), and is usually attributed to the well-known prediction of the spectral index $\alpha_\nu = +1/3$ of the standard thin thermal accretion disc emission (Shakura & Sunyaev 1973; Novikov & Thorne 1973; Frank et al. 1992). This means that it is natural to consider that the flux variability of 3C 323.1 is due to the intrinsic variations of the disc emission itself, in line with other non-blazar quasars; nevertheless, the precise mechanisms for the quasar flux variability are still under debate (see Kokubo 2015, 2016, and references therein). The observed variability time-scale of months to years in 3C 323.1 is also consistent with the variability of the quasar accretion disc emission. As discussed in Section 4, the attribution of the flux variability to the intrinsic disc emission variability, combined with the observed correlated variability between the total flux and the polarized flux, implies that the polarized flux is directly related to the disc emission and does not arise from the optical synchrotron flux contribution.

2.2 Polarimetry data

In this work, we use the three archival polarimetric measurements for 3C 323.1 obtained at different epochs with Bok/SPOL, ESO3.6-m/EFOSC2, and Keck/LRIS. The ESO3.6-m/EFOSC2 observation is V-band imaging polarimetry (Sluse et al. 2005), and the Bok/SPOL and the Keck/LRIS observations are optical spectro-polarimetry (Schmidt & Smith 2000; Kishimoto et al. 2004). The compilation of these polarimetric data from the literature enables to examine the two-epoch spectral variability (Section 3)

[2] For the polarimetric observations for weakly polarized objects, the measurement errors associated with q and u is essentially the same ($\sigma \equiv \sigma_q \simeq \sigma_u$).

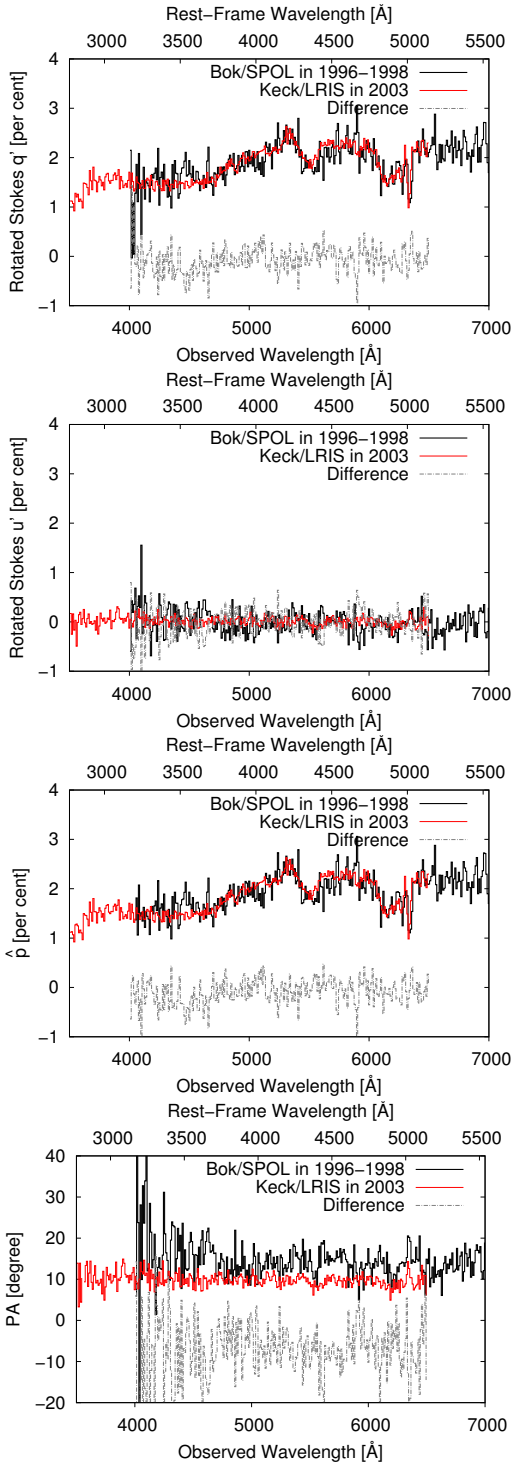

Figure 1. Comparison of the rotated Stokes parameters q' and u', de-biased polarization degree $\hat{p}$, and the polarization position angle (PA) of 3C 323.1 between the spectro-polarimetric measurements of Bok/SPOL (Schmidt & Smith 2000) and Keck/LRIS (Kishimoto et al. 2004). The difference spectra between the two measurements are also plotted. The spectra are binned into common wavelength bins with 10 Å width to allow easy comparison between the two measurements. Note that q' and u' are defined by assuming the systemic PA as PA_c =14.2 deg and 9.6 deg for Bok/SPOL and Keck/LRIS data, respectively.

and the three-epoch V-band variability (Section 4) of the polarimetric properties of 3C 323.1.

The V-band magnitudes of the total flux at the epochs of the three polarimetric measurements are also estimated (Sections 2.2.1 and 2.3). As discussed in Section 4, one of the most important subjects of this work is to examine the correlation between the total flux and the polarized flux light curves, which eventually provides strong constraints on the optical polarization source in 3C 323.1.

Following the same procedure of Kishimoto et al. (2004), we correct the three polarimetric measurements for the effects of Galactic interstellar polarization (ISP). The details of the method of the ISP correction is summarized in Section A. Throughout this paper, the characters with no subscript represent ISP-corrected values unless otherwise stated.

2.2.1 ESO3.6-m/EFOSC2 V-band imaging-polarimetry

Sluse et al. (2005) presented the results of V-band imaging-polarimetry for 3C 323.1 obtained from the 3.6-m telescope at the European Southern Observatory (ESO), La Silla, equipped with the ESO Faint Object Spectrograph and Camera (v.2) (EFOSC2) on the 1st May, 2002 (MJD=52396.3; see also Hutsemékers et al. 2005). As part of this, they took a set of four 60-sec integration images with the half-wave plate position angles of 0.0 deg, 22.5 deg, 45.0 deg, and 67.5 deg.

We downloaded the ESO3.6-m/EFOSC2 imaging-polarimetry data of 3C 323.1 and the associated `BIAS` and `FlatPolIma` frames from the ESO Science Archive Facility (Program ID 68.A-0373). After applying bias and flat corrections, the V-band polarization degree $\hat{p}_V$ and the polarization position angle PA_V of 3C 323.1 were calculated by adopting the aperture photometry and the "ratio" method (e.g., Lamy & Hutsemékers 1999; Bagnulo et al. 2009). By subtracting the instrumental polarization using the values presented in Sluse et al. (2005), we obtained the ISP-uncorrected V-band polarization degree and polarization position angle as $p_{V,\rm uncorr} = 1.14 \pm 0.13$ %, $\hat{p}_{V,\rm uncorr} = 1.13$ % and $PA_{V,\rm uncorr} = 17.88 \pm 3.39$ deg, which are consistent with those reported by Sluse et al. (2005)[3]. By correcting for the Galactic ISP (Section A), we obtain $\hat{p}_V = 1.94$ % and $PA_V = 10.03$ deg (Table 1).

To evaluate the V-band magnitude at the epoch of the EFOSC2 polarimetry measurement, we applied differential photometry by using two field stars (SDSS J154736.44+205141.7 and SDSS J154752.41+204931.8) simultaneously imaged on the same EFOSC2 frames along with 3C 323.1 as reference stars. By using the SDSS g and r-band point spread function (PSF) photometry and the transformation equation by Jester et al. (2005) from the SDSS g and r-band magnitude to V-band magnitude, $V_{Vega} = g - 0.59(g-r) - 0.01$ mag with an uncertainty of 0.01 mag, the V-band magnitudes of SDSS J154736.44+205141.7 and SDSS J154752.41+204931.8 are estimated as $V_{Vega} =$

[3] Sluse et al. (2005) reported the ISP-uncorrected V-band polarization degree and the polarization position angle of 3C 323.1 as $p_{V,\rm uncorr} = 1.15 \pm 0.13$%, $\hat{p}_{V,\rm uncorr} = 1.14$% and $PA_{V,\rm uncorr}$=18±3 deg.

17.0516 mag and V_{Vega} = 16.6971 mag, respectively. For each image, aperture photometry was applied to combine the two orthogonally polarized fluxes of 3C 323.1 and the two reference stars. By adding the 0.01 mag error due to the transformation equation of Jester et al. (2005) to the photometric errors, we evaluated the weighted average magnitude of 3C 323.1 and its uncertainty as $V_{Vega} = 15.7779 \pm 0.0106$ mag or $V_{AB} = 15.7339 \pm 0.0113$ mag, where the AB offset and its uncertainty are taken from Frei & Gunn (1994). The polarimetric and photometric measurements for 3C 323.1 obtained with ESO3.6-m/EFOSC2 are summarised in Table 1.

2.2.2 *Bok/SPOL and Keck/LRIS optical spectro-polarimetry*

3C 323.1 was spectro-polarimetrically observed by Schmidt & Smith (2000) and Kishimoto et al. (2004) during 1996-1998 and 2003, respectively.

Schmidt & Smith (2000) carried out spectro-polarimetric observations of 3C 323.1 at the Steward Observatory 2.3-m Bok Telescope using the SPOL CCD Imaging/Spectropolarimeter (Schmidt et al. 1992) with a low-resolution grating. The observed wavelength range was λ_{obs} = 4000 − 8000 Å. The data presented in Schmidt & Smith (2000) comprise 10 observations from several epochs taken in June 1996 (5 observations) and April 1998 (5 observations), and thus the combined data represent the average polarization properties of 3C 323.1 at MJD∼50235 and 50933. Since the raw Bok/SPOL data of 3C 323.1 are unavailable, in this work, we directly use the combined calibrated polarization spectra of 3C 323.1 presented in Schmidt & Smith (2000), which are kindly provided by G. D. Schmidt and P. S. Smith in electric form. The Galactic ISP is corrected as described in Section A. Following the definition of Kishimoto et al. (2004), the systemic polarization position angle PA_c of 3C 323.1 at the epoch of Bok/SPOL observations is evaluated to be PA_c = 14.2 deg as a weighted average of the PA at the rest-frame wavelength range of 4000-4731Å; thus, the rotated Stoke parameters q' and u' are defined in a coordinate system rotated to $PA_c = 14.2$ deg.

Kishimoto et al. (2004) carried out spectro-polarimetry for 3C 323.1 on the 4th May, 2003 (MJD=52763.6), with the Low Resolution Imaging Spectrometer (LRIS) mounted on the 10-m Keck-I telescope at the W. M. Keck Observatory (Oke et al. 1995; Goodrich et al. 1995; McCarthy et al. 1998), using two grisms of 300 l/mm and 400 l/mm. The observations of 3C 323.1 (76 minutes in total) consisted of two sets of four wave-plate positions (0.0 deg, 22.5 deg, 45.0 deg, and 67.5 deg) × 7.5 minute observations with 300 l/mm and a single set of four wave-plate positions × 4 minute observations with 400 l/mm. As noted in Kishimoto et al. (2004), the observed spectra at the wavelength range at $\lambda_{obs} \gtrsim$6500 Å may be affected by second-order light contamination; therefore, the usable wavelength range for the analysis is λ_{obs} = 3500 − 6500 Å. In this work we use the calibrated polarization spectra of 3C 323.1 presented in Kishimoto et al. (2004), which are kindly provided by M. Kishimoto in electric form (see Kishimoto et al. 2004, for details of the data analysis). The ISP-corrected Keck/LRIS data used in this work are the same with those shown in Figure 9 of Kishimoto et al. (2004). As listed in Table 6 of Kishimoto et al. (2004), the systemic polarization position angle PA_c of 3C 323.1 at the epoch of the Keck/LRIS observation at the rest frame wavelength range of 4000-4731 Å is $PA_c = 9.6$ deg.

Figure 1 shows the ISP-corrected spectra of the rotated Stokes parameters q' and u', de-biased polarization degree $\hat{p}$, and PA of 3C 323.1 obtained with Bok/SPOL (Schmidt & Smith 2000) and Keck/LRIS (Kishimoto et al. 2004). A discussion of the spectral variability of the polarization properties between these two measurements is given in Section 3.2.

To compare the Bok/SPOL and Keck/LRIS spectro-polarimetric measurements with the ESO3.6-m/EFOSC2 V-band imaging-polarimetry data, the V-band polarization degree $\hat{p}_V$ and the polarization position angle PA_V are calculated from the Bok/SPOL and Keck/LRIS spectro-polarimetric data by convolving the total and polarized flux spectra (F_λ, $q_\lambda \times F_\lambda$ and $u_\lambda \times F_\lambda$) with the V-band filter transmission curve taken from Bessell (1990). The errors on $\hat{p}_V$ and PA_V are evaluated as the sample standard deviation of the estimates from the 1000 trials of the Monte Carlo re-sampling of the spectra. The V-band polarimetric properties of 3C 323.1 are summarized in Table 1.

The absolute flux calibration for the total flux (and the polarized flux) spectra of the two spectro-polarimetric measurements is discussed in Section 2.3.

2.2.3 *Note on other historic polarimetric measurements for 3C 323.1*

Other than the three polarimetric data described above, we can find several historic polarimetric measurements in the literature (Stockman et al. 1984; Wills et al. 2011). However, most of these measurements are obtained with white-light (no-filter) configuration, and thus, it is difficult to directly compare them with those obtained with Bok/SPOL, ESO3.6-m/EFOSC2, and Keck/LRIS because of the uncertainty of the wavelength coverage of the data; because the polarimetric properties of 3C 323.1 show wavelength dependence (see Section 3), it is critical for the study of the polarimetric variability to use data taken in the same wavelength range. Also, unlike the three polarimetric data used in this work, it is impossible to evaluate the magnitude values of the total flux of 3C 323.1 at the epochs of these white-light polarimetric data because of lack of referenceable photometric measurements. For these reasons, we do not include the historic white-light polarimetric measurements for 3C 323.1 in the main text; they are instead summarized and discussed in Section B.

2.3 Spectro-photometric flux calibration for the Bok/SPOL and Keck/LRIS data

The absolute flux calibration of the spectroscopic data is generally not quite as accurate as that of the broad-band photometry data. To confidently evaluate the variability of the total and polarized fluxes in 3C 323.1 at the epochs of the spectro-polarimetric observations by Bok/SPOL and Keck/LRIS described in Section 2.2.2, we collect broad-band photometric data from the literature and publicly available

Table 1. Summary of the ISP-corrected V-band polarimetric and photometric values for 3C 323.1.

Date	MJD	Instrument	$\hat{p}_V$[%]	PA_V[deg]	V-band AB mag. of the total flux
1996-06 and 1998-04	50235-50933	Bok/SPOL	2.06±0.01	13.75±0.20	15.8935 ± 0.0358
2002-05-01	52396.3	ESO3.6-m/EFOSC2	1.94±0.13	10.03±3.39	15.7339 ± 0.0113
2003-05-04	52763.6	Keck/LRIS	2.11±0.01	9.61±0.10	15.5838 ± 0.0226

databases (Figure 2), and use them to estimate the V-band magnitude of the total flux.

2.3.1 B- and R-band light curves in 1991-1998

3C 323.1 was photometrically observed for seven years (1991-1998) in the Johnson-Cousins B- and R-band with the Wise Observatory 1-m telescope (see Giveon et al. 1999, for details). The B- and R-band light curves of 3C 323.1 presented by Giveon et al. (1999)[4] are shown in Figure 2. In the same figure, the epoch of Schmidt & Smith (2000)'s Bok/SPOL spectro-polarimetric observations carried out in June 1996 and April 1998 is indicated by vertical bars.

Although there is no available broad-band photometric measurement obtained simultaneously with the Bok/SPOL data, we can infer the broad-band magnitude of 3C 323.1 at the periods of the Bok/SPOL observations from the photometry data of Giveon et al. (1999). We assume that the weighted average of the four R-band measurements of Giveon et al. (1999) from MJD=50174 to 50690, $R_{Vega} = 15.6793 \pm 0.0353$ mag or $R_{AB} = 15.7963 \pm 0.0358$ mag (the AB offset and its uncertainty are taken from Frei & Gunn 1994), represents the magnitude value at the epoch of the observation of Schmidt & Smith (2000). Here, we assume the uncertainty in R_{Vega} as 0.0353 mag, which is derived not from the statistical error but from the sample standard deviation of the four measurements.

The Bok/SPOL total flux spectrum for 3C 323.1 is scaled so that the R_{AB} magnitude calculated by convolving the Bok/SPOL total flux spectrum with the R-band filter transmission curve taken from Bessell (1990) coincides with $R_{AB} = 15.7963$ mag. Then, the polarized flux spectra are defined as the product of the polarization degree spectra in Figure 1 and the scaled total flux spectrum. The V-band magnitude of the scaled total flux Bok/SPOL spectrum is calculated as $V_{AB} = 15.8935$ mag, by using the V-band filter transmission curve taken from Bessell (1990). Because the measurement errors on the Bok/SPOL total flux spectrum are negligible compared to the R-band magnitude uncertainty of 0.0358 mag, we adopt 0.0358 mag as the error of the estimated V-band magnitude. The spectral monochromatic luminosity at 5100 Å is $\lambda L_\lambda(5100\ \text{Å}) = 1.1499(\pm 0.0379) \times 10^{45}$ erg/s. The scaled Bok/SPOL total flux spectrum and the polarized flux spectrum are shown in Figure 3.

It should be noted that, since there is a time separation between the observations from the broad-band measurements in Giveon et al. (1999) and the Bok/SPOL spectro-polarimetric measurements, the spectro-photometric calibration for the Bok/SPOL total and polarized flux spectra should have additional errors due to flux variability during the two Bok/SPOL observations in June 1996 and April 1998. Nevertheless, the magnitude uncertainty of the Bok/SPOL data does not affect the final result of this work in the long term because the observational constraint on the polarization source from the well-correlated total flux and the polarized flux variability (discussed in Section 4) can be verified even from only the two measurements of ESO3.6-m/EFOSC2 and Keck/LRIS whose magnitudes can be confidently evaluated.

2.3.2 SDSS photometry and LINEAR light curve during 2003-2008

3C 323.1 was photometrically observed by the SDSS Legacy Survey, using the SDSS imaging camera mounted on the Sloan Foundation 2.5-m telescope at the Apache Point Observatory (Gunn et al. 1998; York et al. 2000; Gunn et al. 2006). We use the SDSS g-band PSF magnitude of 3C 323.1, $g = 15.5606 \pm 0.0174$ mag, observed on the 12th June, 2004 (MJD=53168.3), retrieved from SDSS Data Release 12 (DR12) SkyServer (Alam et al. 2015). We checked the SDSS photometry flag, and confirmed that the g-band photometry satisfies the "clean photometry" criteria recommended on the SDSS web page[5].

In addition, 3C 323.1 was observed between 2003 and 2008 as part of the Massachusetts Institute of Technology Lincoln Laboratory Lincoln Near-Earth Asteroid Research (LINEAR) survey using the 1-m LINEAR telescope (Stokes et al. 2000; Sesar et al. 2011). The LINEAR observations were carried out with an unfiltered set-up, and the magnitude values stored in the LINEAR Survey Photometric Database [6] are given in the LINEAR recalibrated magnitude (Sesar et al. 2011).

The SDSS photometry data and the LINEAR light curve for 3C 323.1 from MJD=52665 to 54582 are plotted in Figure 2. The multiple LINEAR measurements taken on the same night are binned to a weighted-average magnitude for each observation night. In the same figure, the epoch of the Keck/LRIS spectro-polarimetric observation by Kishimoto et al. (2004) on 4th May, 2003 (Section 2.2.2), is indicated by a vertical bar. As shown in Figure 2, since the LINEAR photometry data were taken approximately simultaneously with both the SDSS data and the Keck/LRIS spectro-polarimetry data, we are able to use the LINEAR photometry data to estimate the broad-band magnitude of 3C 323.1 at the epoch of the Keck/LRIS observation, as described below.

Because quasar spectra are significantly different from

[4] http://wise-obs.tau.ac.il/ givon/DATA/

[5] http://www.sdss.org/dr12/algorithms/photo_flags_recommend/

[6] The LINEAR Survey Photometric Database is available at the SkyDOT Web site (http://skydot.lanl.gov/)

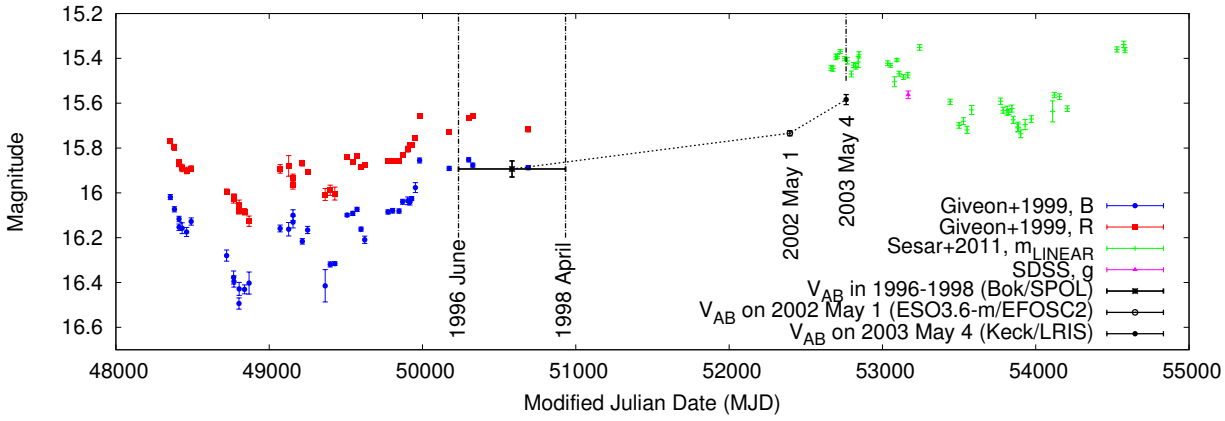

Figure 2. Compilation of the broad-band light curves for 3C 323.1. The B- and R-band light curves at MJD=48355-50690 are taken from Giveon et al. (1999), and the Lincoln Near-Earth Asteroid Research (LINEAR) survey recalibrated magnitudes (m_{LINEAR}) at MJD=52665-54582 are from Sesar et al. (2011). The Sloan Digital Sky Survey g-band photometry at MJD=53168.32 is also plotted. The two periods of the Bok/SPOL spectro-polarimetry and the epoch of the Keck/LRIS spectro-polarimetry are indicated by dashed-dotted vertical bars. The estimated V_{AB} magnitude at the epochs of the three polarimetric measurements (Bok/SPOL, ESO3.6-m/EFOSC2, and Keck/LRIS) is also shown (Table 1; see Section 2.2.1 and Section 2.3 for details).

stellar spectra due to their strong broad emission lines, we do not adopt the LINEAR-to-SDSS photometric transformation equation derived by using the SDSS stellar photometry in Sesar et al. (2011). Instead, we assume that the LINEAR magnitude m_{LINEAR} is related to the SDSS g-band magnitude as $g = m_{LINEAR} + m_{g,0}$. This assumption is justified by the fact that the magnitude difference in the LINEAR measurements between the epochs of the observation of Kishimoto et al. (2004) and the SDSS observation is as small as ∼0.07 mag, and thus the colour variability of 3C 323.1 between these epochs is also expected to be small (see e.g., Schmidt et al. 2012). The LINEAR magnitude at MJD=53165.26 is $m_{LINEAR} = 15.4747 \pm 0.0123$ mag, which can be directly compared to the SDSS photometry obtained three days later, at MJD=53168.3, with the assumption that the quasar flux variability on a time-scale of several days is essentially negligible. From these values, the magnitude shifts are calculated as

$$g = m_{LINEAR} + 0.0859\ (\pm 0.0213) \quad [\mathrm{mag}]. \qquad (1)$$

Keck/LRIS spectro-polarimetry for 3C 323.1 was carried out at MJD=52763.6, and the LINEAR photometry data are available at MJD=52753.35 and MJD=52771.30 as $m_{LINEAR} = 15.4014 \pm 0.0091$ mag and $m_{LINEAR} = 15.4110 \pm 0.0140$ mag, respectively (the weighted-average is $m_{LINEAR} = 15.4043 \pm 0.0076$ mag). With the use of Equation 1, the g-band magnitude of 3C 323.1 at the epoch of the Keck/LRIS observation can be estimated as $g = 15.4902 \pm 0.0226$ mag.

The Keck/LRIS total flux spectrum for 3C 323.1 is scaled so that the g magnitude calculated by convolving the Keck/LRIS total flux spectrum with the g-band filter transmission curve taken from Doi et al. (2010) coincides with $g = 15.4902$ mag. Then, the polarized flux spectra are defined as the product of the polarization degree spectra in Figure 1 and the scaled total flux spectrum. The V-band magnitude of the scaled total flux Keck/LRIS spectrum is calculated as $V_{AB} = 15.5838$ mag, by using the V-band filter transmission curve taken from Bessell (1990). Because the measurement errors on the Bok/SPOL total flux spectrum are negligible compared to the g-band magnitude uncertainty of 0.0226 mag, we adopt 0.0226 mag as the error of the estimated V-band magnitude. The spectral monochromatic luminosity at 5100 Å is $\lambda L_\lambda(5100\ \text{Å}) = 1.7392(\pm 0.0362) \times 10^{45}$ erg/s. The scaled Keck/LRIS total flux spectrum and the polarized flux spectrum are shown in Figure 3.

3 SPECTRAL VARIABILITY OF THE POLARIMETRIC PROPERTIES

In this section, the spectral variability between the two sets of spectro-polarimetry data obtained with Bok/SPOL and Keck/LRIS is examined.

3.1 Spectral variability of the polarization degree and the polarization position angle

Figure 1 clearly shows that, as noted by Schmidt & Smith (2000) and Kishimoto et al. (2004), the polarization degrees (q', u', and $\hat{p}$) at the wavelengths of the BLR emission are significantly diminished, making the polarization degree spectra strongly wavelength-dependent; in particular, the unpolarized "small blue bump", which is composed of the Balmer continuum and the UV Fe II pseudo continuum from the BLR, is responsible for the decrease in the polarization degrees at $\lambda_{\rm rest} < 4000$ Å. Although the spectra of polarization degree do not show strong variability between the two measurements, it should be noted that the polarization degree (i.e., $\hat{p}$) at the rest-frame wavelength range of $\lambda_{\rm rest} \sim 3600$ Å shows variations between the two spectro-polarimetric measurements (see Section 3.2 for details).

Each PA spectrum in the bottom panel of Figure 1 is nearly wavelength-independent. It is clear that, unlike the mainly time-constant polarization degrees, the PA spectra show clear evidence of variability. The difference in the PA evaluated at the rest-frame wavelength range of 4000-4731

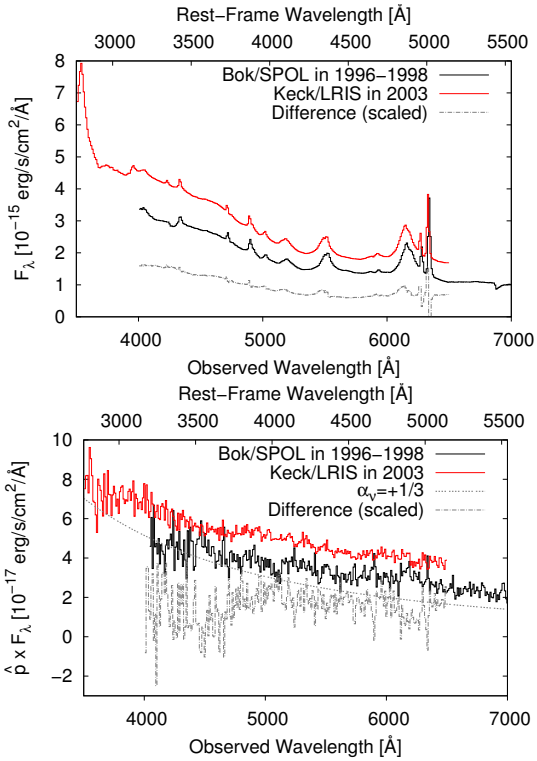

Figure 3. The total flux (top) and the polarized flux spectra (bottom) obtained with Bok/SPOL and Keck/LRIS. Galactic extinction is uncorrected. The arbitrarily-scaled difference spectra between the two measurements are also plotted. The spectra are binned into 10-Å-wide bins. For comparison, a power-law spectrum with $\alpha_\nu = +1/3$ is also plotted in the bottom panel.

Å is $\Delta PA_c = 4.6$ deg, and the PA variability is nearly wavelength-independent (the bottom panel of Figure 1). Because the systematic uncertainties in the grid of polarization standards are at most ~ 1 deg (e.g., Schmidt et al. 1992), the difference in the observed PA between the Bok/SPOL and Keck/LRIS measurements cannot be attributed to errors of the PA calibration by the use of different polarized standard stars, and therefore in this work the observed PA variability is assumed to be the intrinsic variability of the polarization properties of 3C 323.1.

Although PA variability is a general property of the blazar-like synchrotron emission (e.g., Ikejiri et al. 2011), Section 4.1 shows that synchrotron emission is not responsible for the optical polarization observed in 3C 323.1. If we assume that the optical polarization in 3C 323.1 is due to the scattering of the accretion disc continuum, the observed PA variability requires some time-variable axi-asymmetric structure in the scattering region of 3C 323.1, as discussed in detail in Sections 4.2.2 and 4.2.3.

3.2 Spectral variability of the polarized flux

In Figure 3, it is clear that the broad Balmer emission lines seen in the total flux spectra do not appear in either the Bok/SPOL or the Keck/LRIS polarized flux spectra; in other words, the BLR emission is unpolarized in 3C 323.1. As discussed by Kishimoto et al. (2004), the Keck/LRIS polarized flux spectrum ($\hat{p}_\lambda \times F_\lambda$) shows a clear broad absorption-like feature at around $\lambda_{\rm rest} \sim 3600$ Å. Kishimoto et al. (2004) interpreted this feature as the Balmer continuum absorption, but they also noted the possibility that other higher-order Balmer series absorption lines and weak metal absorption lines also contribute to the absorption feature. However, this spectral feature seems to be weak or absent in the Bok/SPOL $\hat{p}_\lambda \times F_\lambda$ spectrum. Interestingly, the detailed shape of the two $\hat{p}_\lambda \times F_\lambda$ spectra also shows evidence of variability at the wavelength range of the Hβ emission line ($\lambda_{\rm rest} \sim$4861 Å); there is a broad absorption-like feature at around the wavelength range of the Hβ emission line in the Keck/LRIS polarized flux spectrum, but it is not clearly seen in the Bok/SPOL polarized flux spectrum. The spectral variability of $\hat{p}_\lambda \times F_\lambda$ at the wavelength ranges of the Balmer continuum and the Hβ emission line can clearly be seen in the difference spectrum shown in the bottom panel of Figure 3.

The spectro-polarimetric variability of 3C 323.1 seen in the $\hat{p}_\lambda \times F_\lambda$ spectra (Figure 3) is very similar to that discovered by Kishimoto et al. (2004) in Ton 202; Kishimoto et al. (2004) have identified spectro-polarimetric variability between the two sets of Keck/LRIS data for Ton 202 obtained in 2002 and 2003 (one year apart), where the Balmer-edge absorption-like feature seen in the polarized flux spectrum in 2002 had disappeared by 2003. Kishimoto et al. (2004) suggested that the spectro-polarimetric variability of Ton 202 might be related to the time-variability of the geometry of the equatorial electron scattering region, but did not discuss how the changes in geometry resulted in the variability of the polarimetric properties around the Balmer continuum and emission lines. Apparently, if the broad absorption features in the polarized flux spectrum are assumed to be intrinsic to the disc thermal emission, it is very difficult to explain reasonably the time-variability of the absorption features by the changes in the geometry of the scattering region alone. Instead, as discussed in detail in Section 4.2.3, we propose that the absorption features are imprinted by an absorbing region with a time-variable structure, which is assumed to be spatially separated from the UV-optical emitting regions of the accretion disc.

In the next section (Section 4), we focus on the V-band polarimetric and photometric variability. As can be clearly seen in Figure 3, the polarized flux variability in the wavelength range of the V-band [$\lambda_{obs} \sim 5000 - 5900$ Å at full width at half maximum (FWHM)] is clearly detected with a high signal-to-noise ratio. It should be noted that the V-band is sampling the rest-frame wavelengths of $\lambda_{\rm rest} \sim 4000 - 4700$ Å, within which the observed flux is dominated by the continuum emission. Therefore, the V-band polarimetric variability mostly reflects the variability of the polarized continuum component. This means that the final results of this work discussed in Section 4 are not affected by the putative changes to the polarization properties around the wavelength range of the Balmer continuum and other recombination lines discussed above.

4 *V*-BAND POLARIMETRIC AND PHOTOMETRIC VARIABILITY AND ITS INTERPRETATION

Figure 4 shows the photometric and polarimetric measurements for 3C 323.1 evaluated in the V-band summarised in Table 1 as a function of time. As shown in the top panel of Figure 4, the polarization degree $\hat{p}$ does not show strong variability during the three observations taken during the period 1996-2003. The total flux F_ν of 3C 323.1 shows $\sim$ 0.3 mag variability during the same period, and the small variability in $\hat{p}$ results in the highly correlated variability between the V-band total flux and the polarized flux ($\hat{p} \times F_\nu$) (the bottom panel of Figure 4).

The middle panel of Figure 4 shows the V-band PA, compared with 3C 323.1's radio jet axis of 20 deg (Kishimoto et al. 2004). As has already been noted in Section 3.1, the observed PA differs between the Bok/SPOL and Keck/LRIS measurements by $\sim$ 4 deg, although the difference between the PA and the radio axis is kept small (i.e., 3C 323.1 remains to be "parallel" polarization).

Below we discuss the geometrical constraints on the optical polarization source in 3C 323.1 derived from the polarimetric and photometric variability seen in Figure 4, and the possible interpretations of the optical polarization mechanism.

4.1 Evidence against the synchrotron origin of the optical polarization in 3C 323.1

As has already been mentioned in Section 3, on the one hand, the Keck/LRIS polarized flux spectrum shows clear broad absorption features, but on the other hand, the Bok/SPOL polarized flux spectrum is almost a smooth power-law spectrum. Based on the Bok/SPOL data, Schmidt & Smith (2000) have suggested that the weak flux contribution of the synchrotron emission to the optical wavelength range can explain the observed optical polarization in 3C 323.1 (see Section 1 for details). Even for the Keck/LRIS data, the synchrotron contribution scenario for the observed polarized flux cannot be ruled out with only the single epoch data; it is possible that the absorption features are imprinted in the intrinsically smooth synchrotron emission spectrum somewhere along the line of sight (Kishimoto et al. 2003).

However, we point out here that the observed polarimetric and photometric variability strongly suggests that the optical synchrotron emission is not the origin of the polarized flux component in 3C 323.1. As shown in Figure 4, the three V-band measurements reveal that both the total and the polarized fluxes vary almost simultaneously; in other words, the polarization degree is nearly time-constant (see also Figure 1). Because the variable component of the total flux must be dominated by the disc continuum emission as discussed in Section 2.1, the observed highly correlated variability between the total and polarized fluxes indicates that the polarized flux has a strong relationship with the accretion disc emission. Therefore, the observation of the polarimetric and photometric variability essentially excludes the possibility that the optical polarization source in 3C 323.1 is the optical synchrotron emission.

In addition to the above mentioned evidence, with reference to the discussion provided in Kishimoto et al. (2003) for the case of Ton 202, we can also confirm the difficulty in attributing the observed polarized flux in 3C 323.1 solely to the flux contribution from the optical synchrotron emission in terms of its core-only radio-loudness. In general, the radio core emission of lobe-dominated quasars becomes optically thin at $\nu > 30$ GHz (Antonucci et al. 1990), and, thus, the ratio of the radio core flux to the optical synchrotron flux (measured at 5000 Å) is expected to be Flux(radio core)/Flux(opt. sync.)$\sim$20,000 by assuming $f_\nu \propto \nu^{-1}$ (Kishimoto et al. 2003). On the other hand, from 3C 323.1's radio-loudness for the core region $R_{\rm core} = 41$ (Schmidt & Smith 2000) and the observed optical polarization degree $p \sim 2\%$, the flux ratio of the radio core flux

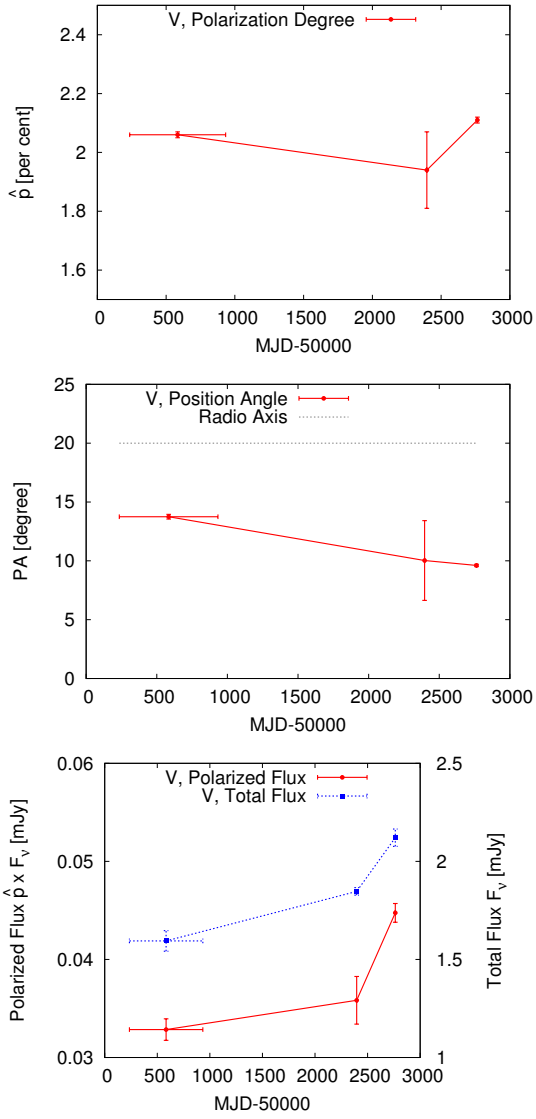

Figure 4. Top and middle: light curves of polarization degree $\hat{p}$ (top panel) and polarization position angle PA (middle panel) of 3C 323.1 given in Table 1. 3C 323.1's radio jet axis of 20 deg (Kishimoto et al. 2004) is indicated as a dotted line in the middle panel. Bottom: the light curves of the V-band polarized flux $\hat{p} \times F_\nu$ (solid line) and total flux F_ν (dotted line) of 3C 323.1; Bok/SPOL in 1996-1998, ESO3.6-m/EFOSC2 on 1st May, 2002, and Keck/LRIS on 4th May, 2003.

to the optical polarized flux is $R_{\rm core}/p \sim 41/0.02$ =2050. Therefore, if we assume that the optical polarized flux in 3C 323.1 originates from the synchrotron emission, the ratio of the radio core flux to the optical synchrotron flux must be Flux(radio core)/Flux(opt. sync.)$\sim 2050 \times p_s$ <2050, where p_s (<1) is the fractional polarization degree of the putative optical synchrotron radiation. The discrepancy in the expected ($\sim$20,000) and required ($\sim 2050 \times p_s$) ratio of the radio core flux to the optical synchrotron flux implies that the amount of flux contribution from the optical synchrotron in 3C 323.1 is too small (by at least an order of magnitude) to account for the observed polarized flux.

Considering the lines of evidence discussed above, we conclude that the optical synchrotron emission is not relevant for the observed optical polarization in 3C 323.1. In Section 4.2, we show that the observed polarimetric and photometric variability properties of 3C 323.1 are consistent with electron scattering from the equatorial scattering region, as proposed by Kishimoto et al. (2004) (see Section 1). However, it is apparently difficult to account for the observed PA variability seen in the middle panel of Figure 4 by the simple equatorial scattering scenario. We attempt to construct a geometrical model to explain all of the observed polarimetric and photometric properties of 3C 323.1 in Section 4.2.

4.2 Constraints on the geometry of the scattering region in 3C 323.1

In this section, we first obtain observational constraints on the radial extent of the scattering region inferred from the polarimetric and photometric variability via causal reasoning, and compare them with the size of the BLR and the dust torus of 3C 323.1. We then propose a geometrical model of the scattering/absorbing regions, which can potentially account for all of the observed polarimetric and photometric properties of 3C 323.1.

4.2.1 Radial extent of the scattering region inferred from the polarimetric and photometric variability

A robust constraint on the geometry of the scattering region can be derived from the highly correlated variability of the V-band total flux and the polarized flux. As has already been pointed out in Section 4.1, the two observations made by ESO3.6-m/EFOSC2 and Keck/LRIS on 1st May, 2002, and 4th May, 2003, respectively (separated by one year, i.e., by 0.8 years in the quasar rest frame), show coordinated variability between the total and polarized fluxes. With the assumption that the polarization in 3C 323.1 is due to scattering of the disc continuum, the time lag between the total flux variation (disc continuum flux) and the polarized flux variation (scattered flux) corresponds to the light travel time across the accretion disc and the scattering region (e.g., Gaskell et al. 2012). Therefore, the observed coordinated variability of the total and polarized fluxes directly constrains the radial distance of the scattering region as

$$R_{\rm sca}(pF\ var.) \quad < \quad 0.8\ [\text{light years}]. \tag{2}$$

On the other hand, within the framework of the equatorial scattering scenario, the PA variability may possibly be interpreted as the change in geometry of the scattering region. Kishimoto et al. (2004) pointed out that the putative equatorial electron scattering region is assumed to be so small in size that its geometrical configuration can be changed within a one-year time-scale. If the putative equatorial electron scattering region in 3C 323.1 is not an axisymmetric disc-like structure but has an axi-asymmetric clumpy density distribution, the PA variability (with little variability in the polarization degree) may be a natural consequence of the orbital or bulk motion of the scattering region (see Section 4.2.3 for details). According to this interpretation, the PA variability observed in 3C 323.1 during the Bok/SPOL and Keck/LRIS observations (the two observations are 5-7 years apart, i.e. a quasar rest frame time-lag of < 6 years) implies that the maximum extent of the size of the scattering region $R_{\rm sca}$ is

$$\begin{aligned} R_{\rm sca}(PA\ var.) \quad &< \quad 6 \times \left(\frac{v_{\rm sca}}{c}\right)\ [\text{light years}] \\ &= \quad 0.20 \times \left(\frac{v_{\rm sca}}{10000 \text{km/s}}\right)\ [\text{light years}] \end{aligned} \tag{3}$$

where $v_{\rm sca}$ represents the typical velocity of the polarization source. If we assume that the polarization source is smaller in size than the BLR, it is reasonable to consider that the value of $v_{\rm sca}$ is larger than the velocity width of the broad emission lines. Since the Hβ broad emission line of 3C 323.1 has an FWHM of $\sim$ 7030 km/s (e.g., Boroson & Green 1992), we take $v_{\rm sca} = 10,000$ km/s to be a reference value in Equation 3.

4.2.2 Comparisons of the radial extent between the polarization source, BLR, and the dust torus

The geometrical constraints on the scattering region $R_{\rm sca}$ derived in Section 4.2.1 should be compared with the radial extent of the accretion disc, BLR, and the dust torus.

Under the assumption of the Shakura & Sunyaev (1973) accretion disc model, the disc radius at which the disc temperature matches the wavelength $\lambda_{\rm rest}$ as $k_B T_{\lambda_{\rm rest}} = hc/\lambda_{\rm rest}$ (h and k_B are the Planck constant and the Boltzmann constant, respectively) can be evaluated as (e.g., Morgan et al. 2010)

$$\begin{aligned} R_{{\rm disc},\lambda_{\rm rest}} \quad &\simeq \quad 0.01\ [\text{light years}] \\ &\times \quad \left(\frac{\lambda_{\rm rest}}{\mu\text{m}}\right)^{4/3} \left(\frac{M_{\rm BH}}{10^9 M_\odot}\right)^{2/3} \left(\frac{L}{\eta L_E}\right)^{1/3}, \end{aligned} \tag{4}$$

where $\eta \equiv L/(\dot{M}c^2)$ indicates the radiative efficiency of the disc. The theoretical values of the radiative efficiency, including general relativistic corrections, range from 6% to 42% as a monotonically increasing function of the black hole spin (e.g., Shapiro & Teukolsky 1983; Frank et al. 1992; Kato et al. 2008). By substituting $\log(M_{\rm BH}/M_\odot) = 9.07$ and $L/L_E = 0.10$ taken from Shen et al. (2011) (see Section 2.1), the disc radius of $\lambda_{\rm rest} = 5100$ Å in 3C 323.1 can be calculated to be within the range

$$R_{\rm disc,5100\text{Å}} = 0.003 - 0.005\ [\text{light years}]. \tag{5}$$

Recent observations of quasar microlensing events and AGN continuum reverberation mapping (e.g., Morgan et al. 2010; Edelson et al. 2015) have revealed that the actual accretion disc sizes in quasars are larger by a factor of $\sim$4 than the size

predicted by the Shakura & Sunyaev (1973) accretion disc model, but even considering such uncertainty, we can conclude from Equation 5 that the accretion disc radii responsible for the optical emission in 3C 323.1 can be regarded as a point source when viewed from the BLR or the dust torus (see below).

The Hβ BLR radius has been determined by reverberation mapping of the broad Hβ emission lines for several tens of AGN/quasars, and can be well expressed as a function of the continuum luminosity as (Bentz et al. 2009)

$$\log R_{\rm BLR}[\text{light days}] = -21.3+0.519\log(\lambda L_{\lambda}(5100\text{Å})\ [\text{erg/s}]) \quad (6)$$

By substituting the monochromatic luminosity $\lambda L_{\lambda}(5100$ Å) at the epochs of Bok/SPOL and Keck/LRIS (see Section 2.3), the BLR radius of 3C 323.1 is found to be in the range of

$$R_{\rm BLR} = 0.33 - 0.41\ [\text{light years}]. \quad (7)$$

The dust reverberation radius of AGN/quasars (e.g., Barvainis 1992; Suganuma et al. 2006; Kishimoto et al. 2011; Koshida et al. 2014, and references therein), which represents the radius of the innermost dust torus, is known to be well represented as a function of the continuum luminosity as $\log R_{\rm dust,\ in}$ [pc] $= -0.88 + 0.5\log(\lambda L_{\lambda}(5500\ \text{Å})/10^{44}$ [erg/s]) (Koshida et al. 2014). By assuming $f_{\nu} \propto \nu^{0}$, this relation can be converted to

$$\log R_{\rm dust,\ in}[\text{light days}] = -19.8+0.5\log(\lambda L_{\lambda}(5100\text{Å})\ [\text{erg/s}]) \quad (8)$$

By substituting the monochromatic luminosity at the epochs of Bok/SPOL and Keck/LRIS, the innermost radius of 3C 323.1's dust torus is in the range of

$$R_{\rm dust,\ in} = 1.47 - 1.81\ [\text{light years}]. \quad (9)$$

Figure 5 shows the comparison of the estimated radius of the BLR and the dust torus innermost radius of 3C 323.1 with the upper limits of the radial extent of the scattering region given in Equations 2 and 3. From this comparison, we can firmly conclude that the scattering region is located inside the dust torus. This means that scattering from regions larger than the dust torus as the dominant polarization mechanism in 3C 323.1 can be completely ruled out. Because the innermost radius of the dust torus corresponds to the sublimation radius of the dust grains (e.g., Kishimoto et al. 2007; Mor & Netzer 2012; Koshida et al. 2014; Netzer 2015), there must be no dust grains inside the dust torus, and thus we can also conclude that electron scattering is the main contributor to the observed optical polarization in 3C 323.1. Moreover, by adopting the size constraint of $R_{\rm sca}(PA\ var.) < 0.20$ light years (Equation 3) at face value, the scattering region should be smaller in size than the BLR, which in turn validates the assumption of the high velocity of the scattering region $v_{\rm sca}$ adopted to derive the constraint on $R_{\rm sca}$ in Equation 3. As has been mentioned in Section 1, the scattering region inside the BLR cannot produce the net polarization of the BLR emission, ensuring the null-polarization of the BLR emission of 3C 323.1. In summary, the constraints on the radial extent of the scattering region in 3C 323.1 obtained in Section 4.2.1 are consistent with the equatorial electron scattering scenario

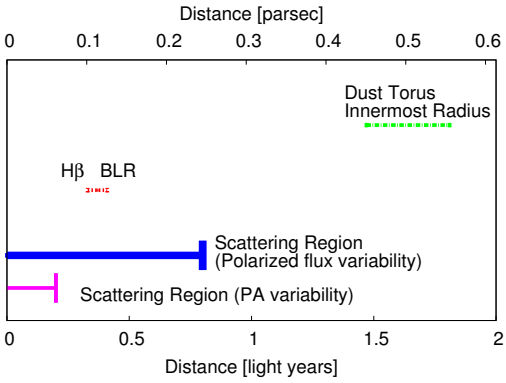

Figure 5. Observational constraints on the radial extent of the scattering region in 3C 323.1. Two independent upper limits on the radial extent of the scattering region are taken from the coordinated variability of the total flux and the polarized flux (Equation 2) and the observed time-scale of the polarization position angle variability (Equation 3 assuming $v_{\rm sca} = 10,000$ km/s). The possible location of the Hβ broad line region (BLR) and the radius of the innermost dust torus are also shown (see Section 4.2.2 for details). Note that the optical emitting region of the accretion disc in 3C 323.1 can be regarded as a central point source if viewed from the BLR and the dust torus (see Equation 5).

proposed by Kishimoto et al. (2003, 2004, 2008b) as the interpretation of the polarization properties of quasars with continuum-confined polarization.

4.2.3 A possible model for the scattering geometry in 3C 323.1

Although the constraints on the radial extent of the scattering region in 3C 323.1 obtained in Section 4.2.2 suggest that the scattering region is located inside the BLR, they do not specify the detailed geometry of the scattering region. Indeed, as was partially discussed above (Sections 3 and 4.2.1), several lines of evidence suggest that the simple assumption that there is an axisymmetric disc-like electron-scattering region that directly scatters accretion disc continuum photons into our line of sight cannot fully account for the observed polarimetric and photometric properties of 3C 323.1.

To infer the true geometrical structure of the inner region of 3C 323.1, we have to take the following observational properties into account:

- As noted in Section 4.2.1, the observed PA variability in 3C 323.1 requires the presence of some axi-asymmetric structure in the scattering region, which changes its geometry on a time-scale of several years;
- The variability of the broad absorption like features in the polarized flux spectra between the Bok/SPOL and the Keck/LRIS observations (Section 3.2) suggests that either (a) the broad absorption features are intrinsic to the accretion disc emission and the strength of the absorption features are time-variable, or (b) there is a high-velocity absorbing region somewhere along the line of sight whose geometry is time-variable;
- As noted in Section 1 (see also Section 2.1), Kokubo (2016) has shown that the spectral shape of the intrinsic accretion disc continuum of 3C 323.1 revealed as the variable

component spectrum is inconsistent with that revealed as the polarized flux spectrum, in that the variable component spectrum is much bluer than the polarized flux spectrum (Figure 3). Within the equatorial scattering geometry, the discrepancy of the spectral shape between the variable and the polarized flux components can only be explained by the above-mentioned scenario (b) as long as the absorbing materials are co-spatial with the equatorial scattering region or located between the accretion disc and the scattering region.

Figure 6 illustrates the geometrical model that can explain the above-mentioned observational properties of 3C 323.1. In this model, an equatorial absorbing region responsible for the broad absorption features (the Balmer continuum, and possibly the Balmer and other weak metal lines, as mentioned in Section 3.2) is located inside (or co-spatial with) the optically-thin equatorial electron scattering region. With this geometrical configuration, the total flux spectrum, and similarly the variable component spectrum, directly reflects the spectral shape of the intrinsic accretion disc continuum, while the polarized flux spectrum shows additional broad absorption features induced by the equatorial absorbing region because the observed polarized light has once passed through the absorbing region. This also indicates that the intrinsic accretion disc continuum is featureless as observed as the variable component spectrum. The geometrical model in Figure 6 is essentially the same as that considered by Kishimoto et al. (2003) and Kokubo (2016) [see the model (a) in Figure 6 of Kishimoto et al. 2003], but in our model the structure of the absorbing/scattering regions is assumed to be axi-asymmetric and time-variable to account for the polarimetric variability observed in 3C 323.1. By requiring that the radial extent of the scattering region is smaller in size than the BLR (i.e., $R_{\rm sca} \lesssim 0.33 - 0.41$ light years; Equation 7), the dynamical time-scale (Kepler orbital time) t_{dyn} of the scattering materials is at most $t_{dyn} \lesssim 88 - 122$ years, assuming $\log(M_{\rm BH}/M_{\odot}) = 9.07$. Therefore, it is possible, in principle, that some dynamical motions (not only the orbital motions but also the radial motions) of the scattering materials gradually modify the net polarization PA on time-scales of several years while keeping the polarization degree nearly constant, as observed in 3C 323.1. the spectral variability of the polarized flux spectra between the Bok/SPOL and Keck/LRIS observations discussed in Section 3.2 can be attributed to some dynamical motions of the absorbing materials.

From the currently available observational constraints alone, it is impossible to specify the physical origins of the absorbing/scattering materials assumed in the proposed model. One promising candidate to produce time-variable inhomogeneous equatorial scattering/absorbing structures is the accretion disc wind, similar to those observed in broad absorption line (BAL) quasars (Elvis 2000; Proga et al. 2000; Young et al. 2007; Matthews et al. 2016), especially Balmer-BAL quasars (Zhang et al. 2015, and references therein). In addition, it may be possible that the accretion disc itself is flaring up at a particular radius (e.g., Lira et al. 2011; Jiang et al. 2016) and that the flared region absorbs some quantity of photons from the inner disc region travelling toward the equatorial direction.

Although this work deals with only a single radio-loud quasar 3C 323.1, we believe that the optical polarization source in other radio-quiet/radio-loud quasars with continuum-confined polarization must be similar to that proposed here considering the similarities of the spectral shape of the polarized flux spectra and the variable component spectra (see Kishimoto et al. 2004, 2008b; Kokubo 2016). Further polarimetric and multi-wavelength monitoring observations for quasars with continuum-confined polarization will eventually clarify the detailed geometry and the true nature of the scattering/absorbing regions in these quasars.

5 SUMMARY AND CONCLUSIONS

We examine the polarimetric and photometric variability of 3C 323.1 by using two optical spectro-polarimetric measurements taken during 1996-1998 (Bok/SPOL) and 2003 (Keck/LRIS) and a V-band imaging-polarimetric measurement taken in 2002 (ESO3.6-m/EFOSC2). The two spectro-polarimetric measurements reveal that the polarimetric properties at the wavelength range of the Balmer continuum and other recombination lines are time-variable, while the polarized degree $\hat{p}$ of the continuum emission is nearly constant (Figures 1 and 3). The V-band polarimetric and photometric measurements (where two of the three measurements are calculated from the two spectro-polarimetry data sets) confirm that the polarization PA is variable on a time-scale of several years (Figure 4). Moreover, the light curves of the V-band total and polarized fluxes show highly correlated variability (Figure 4), indicating that the polarized flux is the scattered disc continuum emission because there is evidence to suggest that the variability of the total flux is due to the intrinsic variability of the accretion disc continuum emission.

The variability time-scales of the PA and the polarized flux introduce the constraint that the polarization source in 3C 323.1 is located inside the BLR (Figure 5), which is consistent with the equatorial electron scattering scenario suggested by Kishimoto et al. (2004). We propose a more sophisticated geometrical model to account for the polarimetric and photometric properties, as well as the variability in behaviour, observed in 3C 323.1. Our model comprises an equatorial absorbing region and an optically-thin equatorial electron-scattering region, which surrounds the UV-optical emitting regions of the accretion disc (Figure 6). The absorbing region is assumed to be co-spatial or smaller in size compared to the scattering region. As schematically shown in Figure 6, this geometrical configuration can explain the discrepancy in the spectral shape of the accretion disc continuum emission in 3C 323.1 revealed as the variable component spectrum (measured by Kokubo 2016) and as the polarized flux spectrum. The structures of both the absorbing region and the scattering region are assumed to be axi-asymmetric and time-variable to account for the variability of the broad absorption features in the polarized flux and the variability of the PA observed in 3C 323.1.

Although the physical origins of the absorbing region and the scattering region are unclear, the accretion disc wind must be a promising candidate to produce the equatorial absorbing/scattering regions around the accretion disc. We believe that the structure of the inner regions of other quasars with continuum-confined polarization must be similar to that proposed here for 3C 323.1, considering the sim-

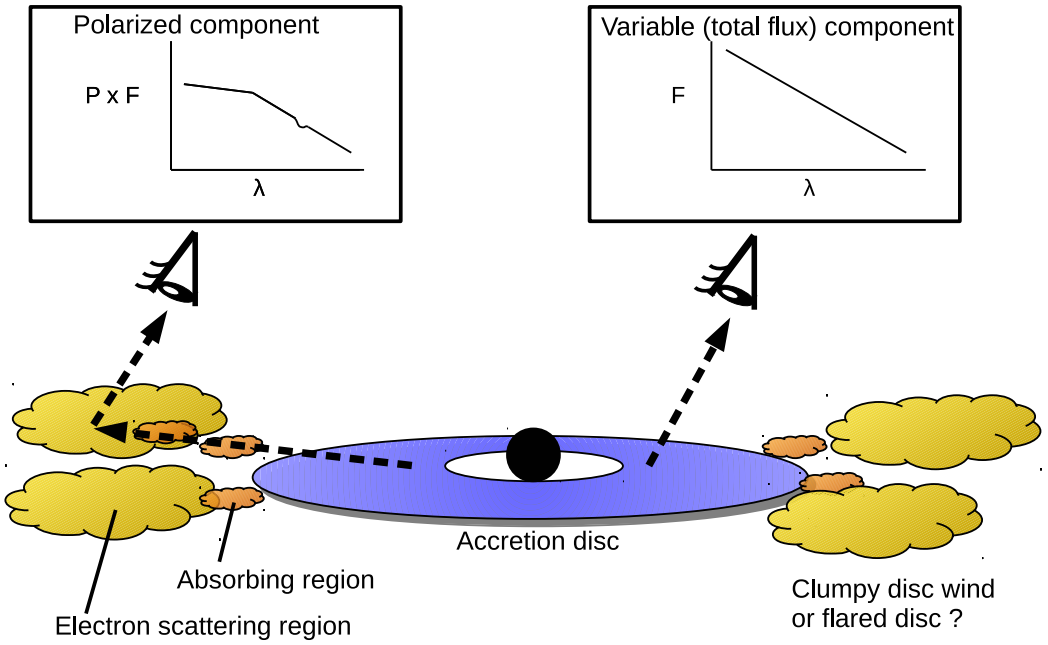

Figure 6. Schematic drawing of the geometrical model for the scattering region of 3C 323.1 and of other quasars with continuum-confined polarization. Note that the broad line region (BLR) is situated outside the optically-thin equatorial electron-scattering region, ensuring the null-polarization of the BLR emission. The variable component spectrum (i.e., the total flux spectrum) directly reflects the spectral shape of the disc continuum emission, while the polarized flux spectrum shows broad absorption features (the Balmer continuum and possibly the Balmer and metal lines; see Figure 3) due to the equatorial absorbing region, which is either co-spatial with the scattering region or located between the accretion disc and the scattering region. The geometric configurations of both the scattering and the absorbing regions are assumed to be axi-asymmetric and time-variable to account for the slight variations of the polarization position angle and the absorption features in the polarized flux observed in 3C 323.1. A clumpy disc wind or flared disc surface may possibly be the physical origin of the absorbing/scattering regions.

ilarities in the spectral shape of the polarized flux spectra and the variable component spectra (see Kishimoto et al. 2004, 2008b; Kokubo 2016). Further polarimetric and multi-wavelength monitoring observations for these quasars will enable us to probe the true nature of the internal structure of these quasars.

ACKNOWLEDGEMENTS

This work was supported by JSPS KAKENHI Grant Number 15J10324. We thank Gary D. Schmidt, Paul S. Smith, and Makoto Kishimoto for providing us with the reduced spectro-polarimetric data presented in Schmidt & Smith (2000) and Kishimoto et al. (2004). This research has made use of NASA's Astrophysics Data System Bibliographic Services. This work is partially based on data obtained from the ESO Science Archive Facility (ESO Programme ID 68.A-0373, PI: D. Hutsemékers).

The LINEAR program is sponsored by the National Aeronautics and Space Administration (NRA No. NNH09ZDA001N, 09-NEOO09-0010) and the United States Air Force under Air Force Contract FA8721-05-C-0002.

Funding for SDSS-III has been provided by the Alfred P. Sloan Foundation, the Participating Institutions, the National Science Foundation, and the U.S. Department of Energy Office of Science. The SDSS-III web site is http://www.sdss3.org/.

SDSS-III is managed by the Astrophysical Research Consortium for the Participating Institutions of the SDSS-III Collaboration including the University of Arizona, the Brazilian Participation Group, Brookhaven National Laboratory, Carnegie Mellon University, University of Florida, the French Participation Group, the German Participation Group, Harvard University, the Instituto de Astrofisica de Canarias, the Michigan State/Notre Dame/JINA Participation Group, Johns Hopkins University, Lawrence Berkeley National Laboratory, Max Planck Institute for Astrophysics, Max Planck Institute for Extraterrestrial Physics, New Mexico State University, New York University, Ohio State University, Pennsylvania State University, University of Portsmouth, Princeton University, the Spanish Participation Group, University of Tokyo, University of Utah, Vanderbilt University, University of Virginia, University of Washington, and Yale University.

REFERENCES

Afanasiev V. L., Shapovalova A. I., Popović L. Č., Borisov N. V., 2015, MNRAS, 448, 2879
Agol E., Blaes O., 1996, MNRAS, 282, 965
Alam S., et al., 2015, ApJS, 219, 12
Angel J. R. P., Stockman H. S., 1980, ARA&A, 18, 321
Antonucci R. R. J., 1983, Nature, 303, 158
Antonucci R., 1988, in Kafatos M., ed., Supermassive Black Holes. pp 26–38

Antonucci R., 2002, in Trujillo-Bueno J., Moreno-Insertis F., Sánchez F., eds, Astrophysical Spectropolarimetry. pp 151–175 (arXiv:astro-ph/0103048)

Antonucci R. R. J., Miller J. S., 1985, ApJ, 297, 621

Antonucci R., Barvainis R., Alloin D., 1990, ApJ, 353, 416

Bagnulo S., Landolfi M., Landstreet J. D., Landi Degl'Innocenti E., Fossati L., Sterzik M., 2009, PASP, 121, 993

Baldi R. D., Capetti A., Robinson A., Laor A., Behar E., 2016, MNRAS, 458, L69

Barvainis R., 1992, ApJ, 400, 502

Batcheldor D., Robinson A., Axon D. J., Young S., Quinn S., Smith J. E., Hough J., Alexander D. M., 2011, ApJ, 738, 90

Bentz M. C., Peterson B. M., Netzer H., Pogge R. W., Vestergaard M., 2009, ApJ, 697, 160

Bessell M. S., 1990, PASP, 102, 1181

Borguet B., Hutsemékers D., Letawe G., Letawe Y., Magain P., 2008, A&A, 478, 321

Boroson T. A., Green R. F., 1992, ApJS, 80, 109

Brindle C., Hough J. H., Bailey J. A., Axon D. J., Ward M. J., Sparks W. B., McLean I. S., 1990, MNRAS, 244, 577

Buisson D. J. K., Lohfink A. M., Alston W. N., Fabian A. C., 2017, MNRAS, 464, 3194

Dennett-Thorpe J., Barthel P. D., van Bemmel I. M., 2000, A&A, 364, 501

Doi M., et al., 2010, AJ, 139, 1628

Edelson R., et al., 2015, ApJ, 806, 129

Elvis M., 2000, ApJ, 545, 63

Frank J., King A., Raine D., 1992, Accretion power in astrophysics.

Frei Z., Gunn J. E., 1994, AJ, 108, 1476

Gallagher S. C., Schmidt G. D., Smith P. S., Brandt W. N., Chartas G., Hylton S., Hines D. C., Brotherton M. S., 2005, ApJ, 633, 71

Gaskell C. M., Goosmann R. W., Merkulova N. I., Shakhovskoy N. M., Shoji M., 2012, ApJ, 749, 148

Giveon U., Maoz D., Kaspi S., Netzer H., Smith P. S., 1999, MNRAS, 306, 637

Goodrich R. W., Cohen M. H., Putney A., 1995, PASP, 107, 179

Goosmann R. W., Gaskell C. M., 2007, A&A, 465, 129

Gunn J. E., et al., 1998, AJ, 116, 3040

Gunn J. E., et al., 2006, AJ, 131, 2332

Hu R., Zhang S.-N., 2012, MNRAS, 426, 2847

Hubeny I., Agol E., Blaes O., Krolik J. H., 2000, ApJ, 533, 710

Hung T., et al., 2016, preprint, (arXiv:1609.06307)

Hutsemékers D., Cabanac R., Lamy H., Sluse D., 2005, A&A, 441, 915

Hutsemékers D., Sluse D., Braibant L., Anguita T., 2015, A&A, 584, A61

Ikejiri Y., et al., 2011, PASJ, 63, 639

Impey C. D., Malkan M. A., Tapia S., 1989, ApJ, 347, 96

Jester S., et al., 2005, AJ, 130, 873

Jiang Y.-F., Davis S. W., Stone J. M., 2016, ApJ, 827, 10

Kato S., Fukue J., Mineshige S., 2008, Black-Hole Accretion Disks — Towards a New Paradigm —

Kellermann K. I., Sramek R. A., Schmidt M., Green R. F., Shaffer D. B., 1994, AJ, 108, 1163

Kishimoto M., Antonucci R., Blaes O., 2003, MNRAS, 345, 253

Kishimoto M., Antonucci R., Boisson C., Blaes O., 2004, MNRAS, 354, 1065

Kishimoto M., Antonucci R., Blaes O., 2005, MNRAS, 364, 640

Kishimoto M., Hönig S. F., Beckert T., Weigelt G., 2007, A&A, 476, 713

Kishimoto M., Antonucci R., Blaes O., Lawrence A., Boisson C., Albrecht M., Leipski C., 2008a, Journal of Physics Conference Series, 131, 012039

Kishimoto M., Antonucci R., Blaes O., Lawrence A., Boisson C., Albrecht M., Leipski C., 2008b, Nature, 454, 492

Kishimoto M., Hönig S. F., Antonucci R., Millour F., Tristram K. R. W., Weigelt G., 2011, A&A, 536, A78

Kokubo M., 2015, MNRAS, 449, 94

Kokubo M., 2016, PASJ, 68, 52

Kokubo M., Morokuma T., Minezaki T., Doi M., Kawaguchi T., Sameshima H., Koshida S., 2014, ApJ, 783, 46

Koshida S., et al., 2014, ApJ, 788, 159

Lamy H., Hutsemékers D., 1999, The Messenger, 96, 25

Lira P., Arévalo P., Uttley P., McHardy I., Breedt E., 2011, MNRAS, 415, 1290

MacLeod C. L., et al., 2016, MNRAS, 457, 389

Marin F., Goosmann R. W., 2013, MNRAS, 436, 2522

Matthews J. H., Knigge C., Long K. S., Sim S. A., Higginbottom N., Mangham S. W., 2016, MNRAS, 458, 293

McCarthy J. K., et al., 1998, in D'Odorico S., ed., Society of Photo-Optical Instrumentation Engineers (SPIE) Conference Series Vol. 3355, Optical Astronomical Instrumentation. pp 81–92

Miley G. K., Hartsuijker A. P., 1978, A&AS, 34, 129

Mor R., Netzer H., 2012, MNRAS, 420, 526

Morgan C. W., Kochanek C. S., Morgan N. D., Falco E. E., 2010, ApJ, 712, 1129

Netzer H., 2015, ARA&A, 53, 365

Novikov I. D., Thorne K. S., 1973, in Dewitt C., Dewitt B. S., eds, Black Holes (Les Astres Occlus). pp 343–450

Oke J. B., et al., 1995, PASP, 107, 375

Pereyra N. A., Vanden Berk D. E., Turnshek D. A., Hillier D. J., Wilhite B. C., Kron R. G., Schneider D. P., Brinkmann J., 2006, ApJ, 642, 87

Plaszczynski S., Montier L., Levrier F., Tristram M., 2014, MNRAS, 439, 4048

Proga D., Stone J. M., Kallman T. R., 2000, ApJ, 543, 686

Richards G. T., et al., 2002, AJ, 123, 2945

Rojas Lobos P. A., Goosmann R. W., Marin F., 2016, preprint, (arXiv:1610.05149)

Ruan J. J., Anderson S. F., Dexter J., Agol E., 2014, ApJ, 783, 105

Schmidt G. D., Smith P. S., 2000, ApJ, 545, 117

Schmidt G. D., Elston R., Lupie O. L., 1992, AJ, 104, 1563

Schmidt K. B., Rix H.-W., Shields J. C., Knecht M., Hogg D. W., Maoz D., Bovy J., 2012, ApJ, 744, 147

Serkowski K., Mathewson D. S., Ford V. L., 1975, ApJ, 196, 261

Sesar B., Stuart J. S., Ivezić Ž., Morgan D. P., Becker A. C., Woźniak P., 2011, AJ, 142, 190

Shakura N. I., Sunyaev R. A., 1973, A&A, 24, 337

Shapiro S. L., Teukolsky S. A., 1983, Black holes, white dwarfs, and neutron stars: The physics of compact objects

Shen Y., et al., 2011, ApJS, 194, 45

Silant'ev N. A., Piotrovich M. Y., Gnedin Y. N., Natsvlishvili T. M., 2009, A&A, 507, 171

Silant'ev N. A., Gnedin Y. N., Piotrovich M. Y., Natsvlishvili T. M., Buliga S. D., 2016, preprint, (arXiv:1606.09050)

Sluse D., Hutsemékers D., Lamy H., Cabanac R., Quintana H., 2005, A&A, 433, 757

Smith P. S., Schmidt G. D., Allen R. G., 1993, ApJ, 409, 604

Smith J. E., Young S., Robinson A., Corbett E. A., Giannuzzo M. E., Axon D. J., Hough J. H., 2002, MNRAS, 335, 773

Smith J. E., Robinson A., Alexander D. M., Young S., Axon D. J., Corbett E. A., 2004, MNRAS, 350, 140

Smith J. E., Robinson A., Young S., Axon D. J., Corbett E. A., 2005, MNRAS, 359, 846

Spergel D. N., et al., 2007, ApJS, 170, 377

Stockman H. S., Angel J. R. P., Miley G. K., 1979, ApJ, 227, L55

Stockman H. S., Moore R. L., Angel J. R. P., 1984, ApJ, 279, 485

Stokes G. H., Evans J. B., Viggh H. E. M., Shelly F. C., Pearce E. C., 2000, Icarus, 148, 21

Suganuma M., et al., 2006, ApJ, 639, 46

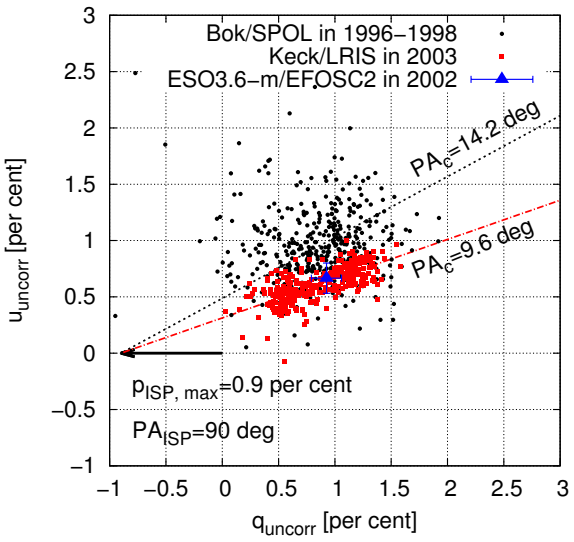

Figure A1. The ISP-uncorrected $q-u$ diagram of the Bok/SPOL and Keck/LRIS spectro-polarimetry data, and the ESO3.6-m/EFOSC2 V-band polarimetry data for 3C 323.1. For the spectro-polarimetry data, each data point is the $q-u$ value at a wavelength bin of 10 Å width. The thick arrow indicates the direction of the ISP polarization, and the dotted lines indicate the ISP-corrected systemic polarization position angles PA_c of the two spectro-polarimetry data evaluated at the rest-frame wavelength range of 4000-4731Å.

Whittet D. C. B., Martin P. G., Hough J. H., Rouse M. F., Bailey J. A., Axon D. J., 1992, ApJ, 386, 562
Wills B. J., Wills D., Breger M., 2011, ApJS, 194, 19
Wright E. L., 2006, PASP, 118, 1711
York D. G., Adelman J., Anderson Jr. J. E., Anderson S. F., Annis J., SDSS Collaboration 2000, AJ, 120, 1579
Young S., Axon D. J., Robinson A., Hough J. H., Smith J. E., 2007, Nature, 450, 74
Zakamska N. L., et al., 2005, AJ, 129, 1212
Zhang S., et al., 2015, ApJ, 815, 113

APPENDIX A: CORRECTING FOR THE EFFECTS OF THE GALACTIC ISP

Kishimoto et al. (2004) pointed out that the observed optical polarization of 3C 323.1 is affected by a non-negligible amount of the Galactic ISP. The wavelength dependence of the ISP linear polarization can be described by the empirical formula (e.g., Serkowski et al. 1975)

$$p_{\rm ISP} = p_{\rm ISP,\ max} \exp\left[-K \ln^2\left(\frac{\lambda_{\rm max}}{\lambda}\right)\right], \quad \text{(A1)}$$

where $K = 0.01 + 1.66\lambda_{\rm max}$ (Whittet et al. 1992). In this work, we adopt the ISP parameters of $p_{\rm ISP,\ max} = 0.90\%$ and $\lambda_{\rm max} = 5570$Å, and the ISP position angle of $PA_{\rm ISP} = 90$ deg derived by Kishimoto et al. (2004) for 3C 323.1. $PA_{\rm ISP} = 90$ deg means that the ISP vector in the direction of 3C 323.1 is parallel to the q-axis in the $q-u$ plane, and thus, the ISP correction for q and u can be described as $q = q_{\rm uncorr} + p_{\rm ISP}$ and $u = u_{\rm uncorr}$, where $q_{\rm uncorr}$ and $u_{\rm uncorr}$ represent the ISP-uncorrected values (see Figure A1).

Figure A1 shows the ISP-uncorrected $q-u$ (i.e., $q_{\rm uncorr} - u_{\rm uncorr}$) diagram of the Bok/SPOL and Keck/LRIS spectro-polarimetry data, and the ESO3.6-m/EFOSC2 V-band imaging-polarimetry data for 3C 323.1. In Figure A1, the ISP vector of $p_{\rm ISP} = 0.9\%$ is shown as a representative value, but it should be noted that the actual ISP correction is slightly wavelength-dependent (Equation A1). The ISP correction leads to a shift of the origin of the intrinsic polarization vector to $(q_{\rm uncorr}, u_{\rm uncorr}) = (-p_{\rm ISP}, 0)$, and the ISP-corrected PA is defined as half the geometrical angle between the q-axis and lines passing through the shifted origin and data points. As indicated in Figure A1, the Keck/LRIS data points are linearly aligned along the vector of $PA_c = 9.6$ deg, meaning that the ISP-corrected PA of 3C 323.1 is nearly wavelength-independent (Figure 1; Kishimoto et al. 2004). As we can see in Figure 1, the ISP-corrected PA spectrum obtained with Bok/SPOL is also nearly wavelength-independent.

APPENDIX B: HISTORIC WHITE-LIGHT POLARIMETRIC MEASUREMENTS FOR 3C 323.1

Historic polarimetric measurements for 3C 323.1 presented in Stockman et al. (1984) and Wills et al. (2011) are summarized in Table B1. It should be noted that, unlike the Bok/SPOL, ESO3.6-m/EFOSC2, and Keck/LRIS polarimetric measurements given in Table 1, it is impossible to estimate the V-band magnitudes of the total flux at each epoch of the polarimetric measurement summarized in Table B1 because referenceable photometric measurements at these epochs are not available in the literature. Also, we do not correct for the Galactic ISP for these historic data, because it is difficult to evaluate the ISP strength from Equation A1 due to the uncertainty of the wavelength coverage (see below).

In Figure B1, the time variation of the ISP-uncorrected $\hat{p}$ and PA of 3C 323.1 as given in Table B1 are plotted, where different symbols indicate different filter configurations. We also plot the ISP-uncorrected $\hat{p}_V$ and PA_V derived from the Bok/SPOL, ESO3.6-m/EFOSC2, and Keck/LRIS data in the same figure. As has already been pointed out in Section 2.2.3, the historic polarimetric measurements summarized in Table B1 are not taken with standard photometric filter system. Considering the uncertainty of the wavelength coverage of each measurement, what we can only infer about the variability of $\hat{p}$ in 3C 323.1 from the historic (mostly white-light) polarimetric data in Table B1 is that there is no evidence to support the existence of strong variability of $\hat{p}$ for the last several decades. On the other hand, since the wavelength-dependence of PA of 3C 323.1 is relatively weak, it may be valid to conclude that the PA has been showing time-variability. As discussed in Section 4, the variability of PA is observed even when we focus only on the V-band measurements presented in Table 1, and thus the historic PA data are supporting the discussion given in the main text that the PA variability has real physical origin intrinsic to the innermost scattering structure of 3C323.1.

This paper has been typeset from a TEX/LATEX file prepared by the author.

Table B1. Historic white-light and filtered polarimetric measurements for 3C 323.1. The Galactic ISP is uncorrected.

Date	MJD	Filter	$\hat{p}_{\rm uncorr}$[%]	$PA_{\rm uncorr}$[deg]	Reference
1977-09-11	43397	None (Steward)	1.63±0.24	16±4	Stockman et al. (1984)
1978-05-05	43633	None (UAO)	2.01±1.25	—	Stockman et al. (1984)
1979-04-02	43965	None (Steward)	1.48±0.30	19±6	Stockman et al. (1984)
1979-05-22	44015	None (Steward)	1.01±0.20	4±5	Stockman et al. (1984)
1979-05-22	44015	$CuSO_4$ + B-390 (Steward)	0.78±0.24	−8±8	Stockman et al. (1984)
1979-05-22	44015	RG715 (Steward)	0.55±0.26	−4±12	Stockman et al. (1984)
1980-03-15	44313	None (Steward)	1.42±0.30	8±6	Stockman et al. (1984)
1990-02-26	47948	None (McDonald)	1.02±0.13	28.3±3.6	Wills et al. (2011)

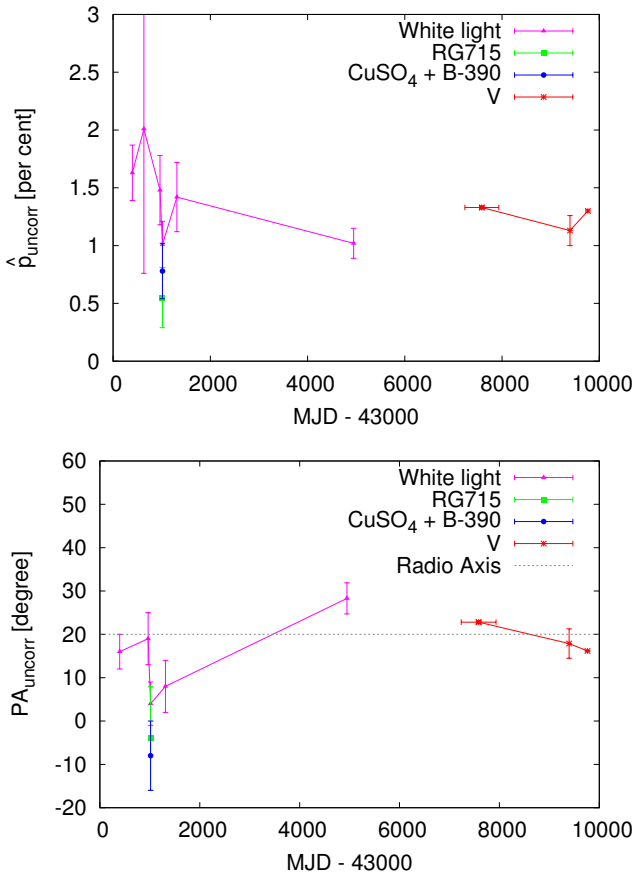

Figure B1. The time variation of the ISP-uncorrected $\hat{p}$ and PA of 3C 323.1 in 1977-2003. 3C 323.1's radio jet axis of 20 deg (Kishimoto et al. 2004) is indicated as a dotted line in the bottom panel.